SCIENCE CHINA
Chemistry

•ARTICLES•

June 2019 Vol.62 No.6: 753–760
https://doi.org/10.1007/s11426-018-9447-4

One-dimensional π-d conjugated coordination polymers: synthesis and their improved memory performance

Xue-Feng Cheng[1], Jie Li[2], Xiang Hou[1], Jin Zhou[1], Jing-Hui He[1*], Hua Li[1], Qing-Feng Xu[1], Na-Jun Li[1], Dong-Yun Chen[1] & Jian-Mei Lu[1*]

[1]*College of Chemistry, Chemical Engineering and Materials Science, Soochow University, Suzhou 215123, China;*
[2]*Shanghai Institute of Measurement and Testing Technology, Shanghai 201203, China*

Received December 21, 2018; accepted February 25, 2019; published online March 28, 2019

Multilevel resistance random access memories (RRAMs) are intensively studied due to their potential applications in high density information storage. However, the low ternary device yields and high threshold voltages based on current materials cannot meet the requirement for applications. Improvement via material innovation remains desirable and challenging. Herein, five one-dimensional conjugated coordination polymers were synthesized via the reaction between metal ions (Zn^{2+}, Cu^{2+}, Ni^{2+}, Pt^{2+} and Pd^{2+}) and 2,5-diaminobenzene-1,4-dithiol (DABDT) and fabricated into RRAM devices. The as-fabricated ternary memories have relatively low threshold voltages (V_{th1}: −1 to −1.4 V, V_{th2}: −1.8 to −2.2 V). Their ternary device yields were improved from 24% to 56%. The first and the second resistance switches are interpreted by the space charge limited current (SCLC) and grain boundary depletion limited current (GBLC) modes, respectively. The Pd-DABDT, which is of planar structure, smaller band gap and better crystallinity than others, shows the best performance among these five polymers. Our work paves a simple and efficient way to optimize the performance of ternary RRAM devices employing one-dimensional hybrid materials.

one-dimensional coordination polymer, resistive random access memory, ternary device yield, low threshold voltages, d-π conjugation

Citation: Cheng XF, Li J, Hou X, Zhou J, He JH, Li H, Xu QF, Li NJ, Chen DY, Lu JM. One-dimensional π-d conjugated coordination polymers: synthesis and their improved memory performance. *Sci China Chem*, 2019, 62: 753–760, https://doi.org/10.1007/s11426-018-9447-4

1 Introduction

The rapid development of modern technologies results in the explosive growth of information. Traditional techniques cannot meet the increasing data storage requirement, which urges the development of new ultra-high-density data storage techniques [1–4]. Resistive random access memories (RRAM) rise as a competitive candidate for the next generation of ultra-high-density data storage techniques due to their low cost, simple structure, easy processability, low power consumption and layer by layer stacking ability [5–13]. In addition, multiple resistance states could be implemented in one RRAM cell with typical electrode/active layer/electrode structure, increasing the storage capacity significantly [14–20].

In the typical indium tin oxide (ITO)/active layer/Al sandwich-like structure of an RRAM, the choice of active layer materials governs the memory behavior. Conjugated organic materials, including small molecules and polymers, have been widely used in RRAM devices and perform binary, ternary, or quaternary memory behaviours [6,15,16,19–21]. However, they have low ternary device yield, high threshold voltages, and environmental and thermal instabilities suffering from intrinsically weak intermolecular-interaction of organic materials. Our previous work proposed to use one-dimensional (1D) d-π conjugated coordination

*Corresponding authors (email: Jinghhe@suda.edu.cn; lujm@suda.edu.cn)

polymers (CCPs) as a typical inorganic-organic hybrid material to partially address these performance issues, taking the advantages of structural tailorability of organic molecules and high thermal/environmental stability of inorganic materials together [22]. However, the ternary device yields and threshold voltages are still unsatisfied and have room to improve towards potential applications. Further improvement via formula design of 1D CCPs remains both attractive and desirable.

It is widely accepted that the charge transportation in the film plays an important role in RRAM performance [23–28]. The charge transportation could be improved from tuning the crystallite orientation and band gap of organic materials. For highly-oriented crystallites in the active layer of RRAMs, the ordered connection between grains and fewer defects in the films facilitate the charge transportation [24]. On the other hand, the narrower bandgap contributes to a much faster charge hopping rate according to Marcus transportation theory [29–31]. The band gaps of conjugated molecules can be reduced by increasing chain planarity which helps electrons delocalise much more efficiently. In addition, the choices on metal-ligand species are also important as their coordination bond also influence the band gaps.

In this work, we achieved ternary memory behaviour with low threshold voltages and improved ternary device yields from new 1D conjugated coordination polymers. Five 1D conjugated coordination polymers were synthesized via the coordination reaction between M^{2+} (M=Zn, Cu, Ni, Pt, or Pd) and 2,5-diaminobenzene-1,4-dithiol (DABDT). The RRAM devices fabricated from these five 1D CCPs have their first/second threshold voltages as low as −1.0 V/−1.8 V and ternary device yields varying from 24% to 56%. We demonstrated that through altering the central metal ions, planar chains, smaller band gaps, and better crystallinities were gradually achieved, finally resulting in the better memory performance. Our work paves a simple and efficient way in which to improve performance for ternary RRAM devices from lower-dimensional hybrid materials.

2 Experimental

2.1 Materials

2,5-Diaminobenzene-1,4-dithiol, zinc dichloride, copper sulfate pentahydrate, nickel dichloride hexahydrate, platinum dichloride, palladium dichloride were purchased from Adamas or Energy Chemical Co., Ltd. (China) and used without further purification. All solvents were purchased from Sinopharm Chemical Reagent Co., Ltd. (China).

2.2 Synthesis of M-DABDT

DABDT (1 mmol, 245.2 mg) was dissolved with 50 mL dimethylformamide (DMF) in a 100 mL two-necked flask and stirred with dried N_2 purging for 5 h. Then metal(II) salts (1 mmol, $ZnCl_2$/$CuSO_4\cdot5H_2O$/$NiCl_2\cdot6H_2O$/$PtCl_2$/$PdCl_2$) were dissolved in 50 mL of deionized water and added dropwise into the DABDT solution at 0 °C. The pH of the mixture was adjusted to 7.0 by adding ammonium hydroxide, followed by stirring of the mixture at room temperature for 6 h. After completion of the reaction, the solvent was evaporated under vacuum and the residue was washed by deionized water and acetone for three cycles. Finally, the solid was dried under vacuum at 70 °C for 12 h.

2.3 Fabrication of devices

ITO glasses were washed by detergent and deionized water, acetone and ethanol in ultrasonication for 10 min, respectively. Then the M-DABDT solutions (DMSO and DMF mixed solvent with volume ratio 1:1) were spin-coated on ITO glass substrates with 500 r/min for 5 s, followed by 1500 r/min for 15 s, respectively. Then the film was dried at 70 °C under vacuum for 4 h. Cover the films with shadow masks and fabricate the Al top electrode by vacuum thermal evaporation.

2.4 Measurements and general methods

UV-Vis absorption spectra were obtained from Shimadzu UV-3600 spectrometer (Japan). Shimadzu XRD-600 spectrometer with a Cu Kα monochromatic radiation source at 40 kV and 30 mA was used to obtain X-ray photoelectron spectroscopy (XPS) diffraction patterns. Thermogravimetric analysis (TGA) was performed on a Perkin-Elmer Diamond TG/DTA instrument (USA) under the protection of nitrogen gas with a heating rate of 10 °C/min. Scanning electron microscopy images were taken using a Hitachi S-4700 scanning electron microscope (Japan). Current-voltage (*I*-*V*) curves of devices were measured by a Keithley 4200-SCS semiconductor analyzer (USA) in a voltage sweep mode. The testing of the pulse iteration used −0.5 V stress with a pulse/relaxation duration period of 1/1 μs, respectively. Cyclic voltammograms were collected by a CorrTest CS Electrochemical Workstation analyzer at a sweep rate of 100 mV/s in 0.1 M solution of tetrabutylammonium hexafluorophosphate ($TBAPF_6$) with mixed solvent (DMSO/DMF, *v*/*v*=1:1).

3 Results and discussion

Five d-π conjugation polymers (Zn-DABDT, Cu-DABDT, Ni-DABDT, Pt-DABDT, and Pd-DABDT) were synthesized via the coordination reactions between the metal(II) ions and 2,5-diaminobenzene-1,4-dithiol (DABDT) in diluted am-

monia solutions (Figure 1). After several hours of reaction, the products were washed by deionised water and acetone for three cycles. Brown Zn-DABDT and other black 1D CCPs powdered products were obtained after vacuum-drying at 70 °C for 12 h (Figure S1, Supporting Information online) [32]. The existence of metal(II) ions, C, N, and S in these 1D CCPs could be confirmed by XPS spectra. The elemental mapping images of 1D CCP powders show the uniform distribution of each element (Figures S2–S6). Additionally, two characteristic N–H stretching modes (3393 and 3277 cm^{-1}) from $–NH_2$ appeared in the IR spectra of DABDT (Figure 2(a)) and disappeared in all 1D CCPs whereas the vibrations of the benzene ring remained (1450–1600 cm^{-1}, Figure 2(b)), indicating the transformation of $–NH_2$ to –NH– in all products.

In order to investigate the molecular geometries of these 1D CCPs, we used density functional theory (DFT) calculations to simulate the oligomer chains with a degree of polymerisation increasing from 1 to 4 (Figure 3, Figures S3, S7–S10). According to the simulation, Ni-DABDT, Pt-DABDT, and Pd-DABDT chains have rigid and coplanar geometries, while the ligand plane of Zn-DABDT and Cu-DABDT twists by 97.16° and 12.02°, respectively (Figure S11). The coordination bonds formed mainly from overlapping of the delocalised π orbital of DABDT and the d orbital of metal(II) ions. The square planar coordination nature of d^8 metal ions Ni^{2+}, Pt^{2+}, and Pd^{2+} resulted in the rigid and planar geometries of their polymer chains. In contrast, for Cu^{2+} and Zn^{2+}, tetrahedral coordination formed with four ligands. Therefore, Zn-DABDT and Cu-DABDT chains twisted and the conjugation of these two CCPs were weaker than those of the other three CCPs, which could be observed from their frontier orbitals.

From the UV-Vis absorption spectra of these 1D CCPs (Figure 2(d)), the onsets of absorption peaks were 516 nm (Zn-DABDT), 847 nm (Cu-DABDT), 920 nm (Pd-DABDT), 1162 nm (Ni-DABDT) and 1169 nm (Pt-DABDT), corresponding to band gaps of 2.40, 1.46, 1.35, 1.07, and 1.06 eV, respectively. The band gaps of the planar structure 1D CCPs are smaller than those of the two twisted 1D CCPs, consistent with our theoretical simulation. The electrochemical properties of each 1D CCP were also investigated. The onset oxidation potentials (*E*onset OX) of 1D CCPs were found to be: 0.47 eV (Zn-DABDT), 0.14 eV (Cu-DABDT), 0.53 eV (Pd-DABDT), 0.50 eV (Ni-DABDT), and 0.40 eV (Pt-DABDT) as evinced by cyclic voltammogram data (Figure S12). For all 1D CCPs, the hole injection barriers were smaller than the electron injection barriers (Table 1). Therefore, the charge transportation in all 1D CCP films was mainly hole-dominated.

X-ray diffraction (XRD) testing was conducted to investigate the crystallinities of these 1D CCPs. The M-DABDT film on ITO substrates showed no diffraction peaks except those peaks arising from the ITO substrates themselves (Figure S13), caused by the relatively poor crystallinity of these 1D CCPs. Therefore, powder-state XRD assays were further conducted. Zn-DABDT, Cu-DABDT, and Pd-DABDT CCP powders show good crystallinities with several sharp peaks, such as those at 2θ=18.4°, 20.6°, and 26.9° (d=2.44, 2.19 and 1.70 Å) for Zn-DABDT; 20.4°,

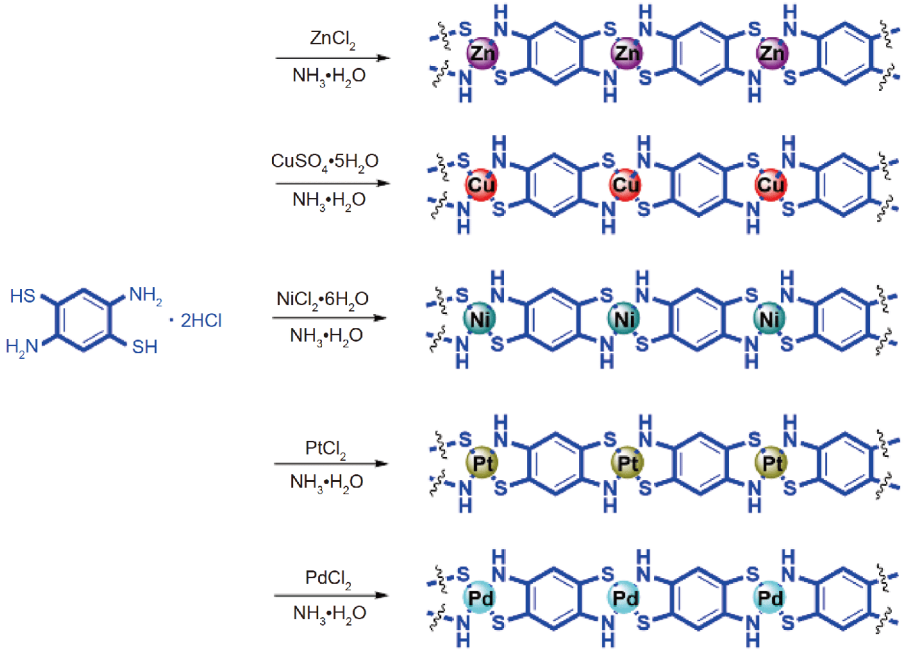

Figure 1 Synthetic routes of M-DABDT (M: Zn, Cu, Ni, Pt, Pd). Different metal ions are labeled by unique colors, which are also used in other figures hereafter (color online).

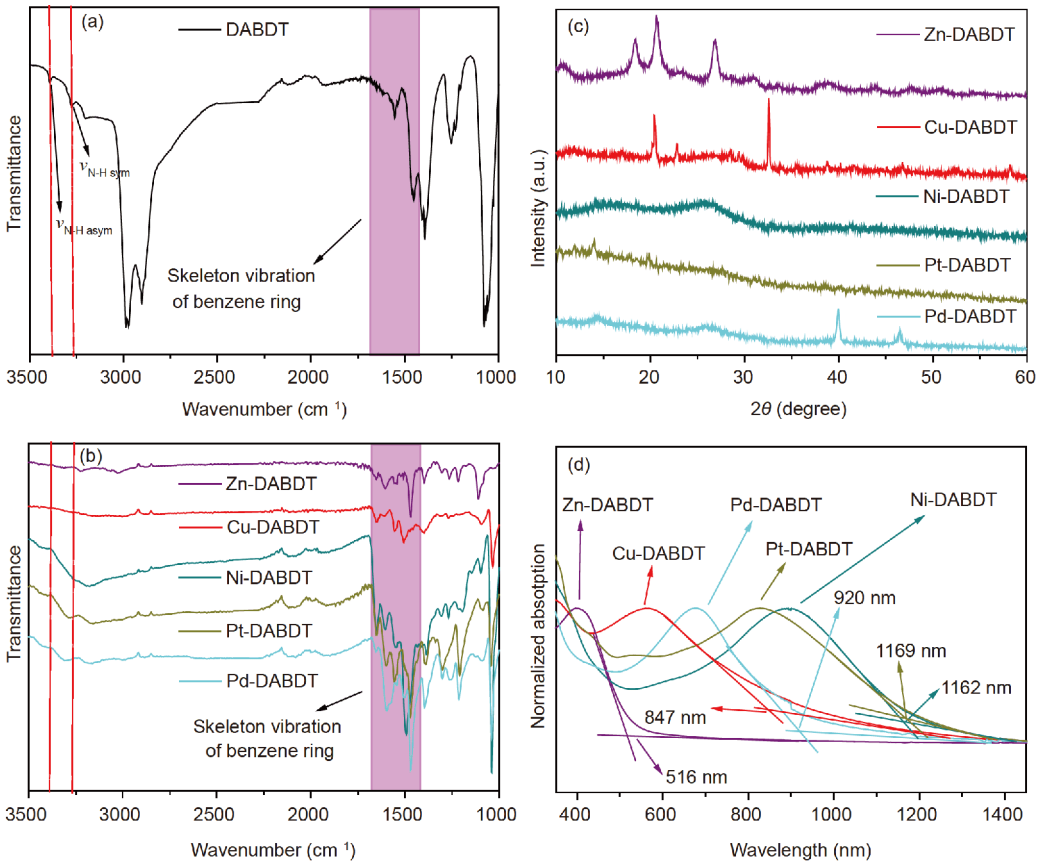

Figure 2 Fourier transfer infrared spectra of (a) DABDT, and (b) M-DABDT. (c) X-ray diffraction patterns of M-DABDT powder. (d) UV-Vis spectra of M-DABDT solution (DMSO/DMF, *v*/*v*=1:1). M: Zn, Cu, Ni, Pt and Pd (color online).

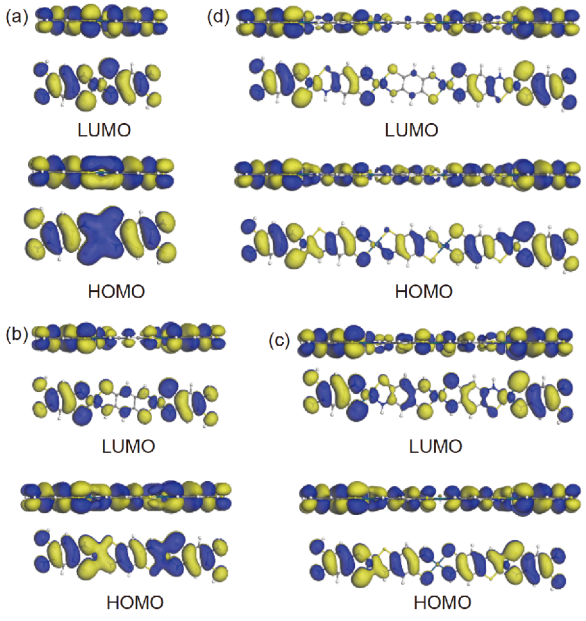

Figure 3 The isosurfaces of the highest occupied orbitals (HOMOs) and lowest unoccupied orbitals (LUMOs) of Pd-DABDT oligomers with their Pd(II) core number increasing from 1 to 4. (a) $Pd_{1D}ABDT_2$; (b) Pd_2-$DABDT_3$; (c) Pd_3-$DABDT_4$; (d) Pd_4-$DABDT_5$. In all plots, isovalue= 0.01 e/Å^3 (color online).

22.8°, and 32.6° (*d*=2.21, 1.99 and 1.43 Å) for Cu-DABDT; and 39.3° and 46.5° (*d*=1.22 and 1.06 Å) for Pd-DABDT. On the other hand, diffraction peaks for Pt-DABDT CCP powder were weak and those for Ni-DABDT CCP powder were broader [33–35]. Thus, the crystallinity of Pt-/Ni-DABDT CCP powder was lower than that of other CCP powders. From the thermogravimetric analysis, our 1D CCP powders could sustain a temperature of at least 170 °C without obvious decomposition, indicating their good thermal stability (Figure S14).

The availability as RRAM active materials of these 1D CCPs was tested via fabrication of sandwich-like RRAM devices (Figure 4(a)) consisting of ITO-coated glass (bottom electrode), 1D CCPs (active layer, approximately 145 nm thick, Figure S15) and Al (top electrode). Our 1D CCP powders are soluble in mixed solvent (DMSO/DMF, *v*/*v*=1:1) under sonication. Therefore, a spin-coating method was chosen to prepare 1D CCP films on the clean ITO glasses. The films were then covered with shadow masks and the Al top electrodes were prepared through vacuum thermal evaporation of Al.

The typical ternary memory behaviours of Pd-DABDT-based memory devices are shown in Figure 4(b). A negative voltage sweep of the device from 0 to −3 V (sweep 1) causes

Table 1 Optical and electrochemical properties of M-DABDT (M: Zn, Cu, Ni, Pt and Pd)

Molecule	λ_{onset} (nm)	E_g [a] (eV)	HOMO [b] (eV)	LUMO [c] (eV)	Hole injection [d] (eV)	Electron injection [e] (eV)
Zn-DABDT	516	2.40	−4.89	−2.49	0.09	1.81
Cu-DABDT	847	1.46	−4.56	−3.10	0.24	1.20
Ni-DABDT	1162	1.07	−4.92	−3.85	0.12	0.45
Pt-DABDT	1169	1.06	−4.82	−3.76	0.02	0.54
Pd-DABDT	920	1.35	−4.95	−3.60	0.15	0.70

a) Estimated from the onset of UV-Vis absorption: $1240/\lambda_{onset}$; b) HOMO=−[$E_{onset\ OX}$+4.8–$E_{Ferrocene}$]; c) LUMO=HOMO+E_g; d) the difference between the work function of ITO and the HOMO energy level; e) the difference between the LUMO energy level and the work function of Al.

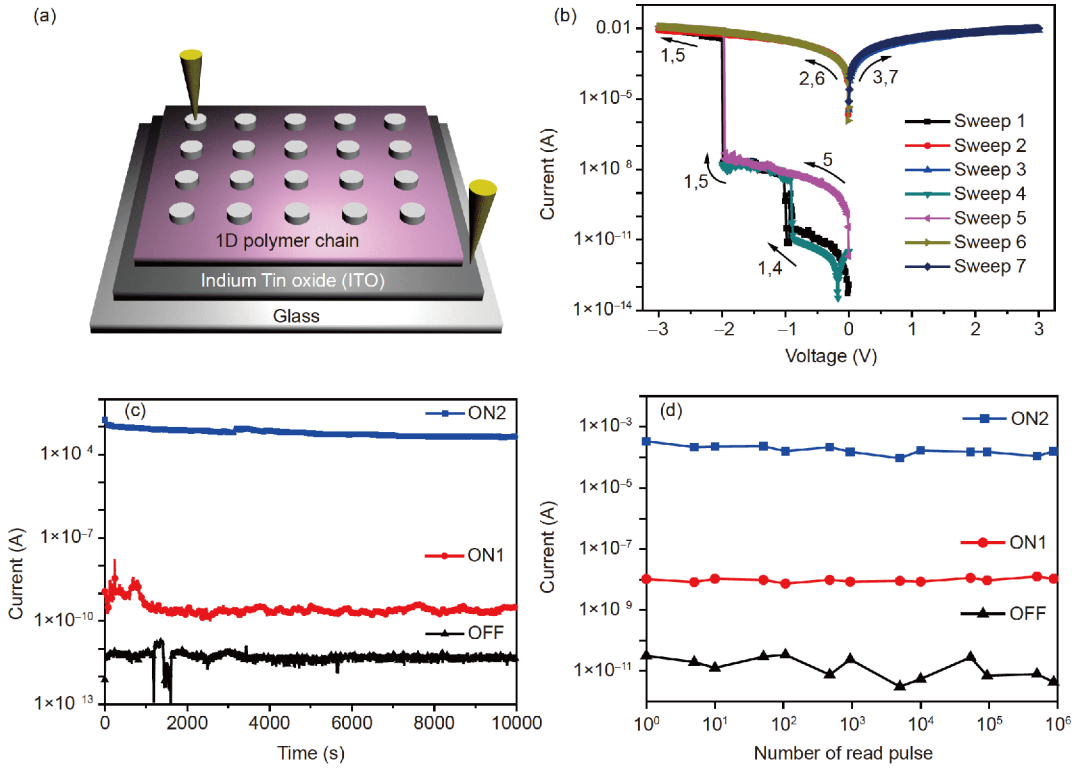

Figure 4 (a) Typical sandwiched structure of memory device; (b) characteristic current-voltage (*I-V*) curves of Pd-DABDT based devices; (c) retention stability of Pd-DABDT based device in OFF, ON1 and ON2 states with the operation voltage of −0.5 V; (d) iteration stability of Pd-DABDT based device under −0.5 V stress with a pulse/relaxation duration period of 1/1 μs, respectively (color online).

an abrupt jump from its low-conductive (OFF) state to an intermediate-conductive (ON1) state at −1.2 V (V_{th1}, representing the average value of fifty devices). Another jump from an intermediate-conductive state to a high-conductive (ON2) state occurs at −2.0 V (V_{th2}, representing the average value across fifty devices). These three states with different current levels could be regarded as three data storage states: "0" (OFF), "1" (ON1), and "2" (ON2). Once the memory device was written into its ON2 state, neither negative (sweep 2) nor positive (sweep 3) voltage sweeps could erase the device to the ON1 or OFF states, therefore, the Pd-DABDT-based device performs ternary Write-Once-Read-Many-Times (WORM) type memory behaviour.

When a lower negative voltage (from 0 to −2 V) was applied to another cell of a Pd-DABDT-based device (sweep 4), only one jump occurred from the OFF state to an ON1 state. The other jump from the ON1 to ON2 state could be observed in the next sweep from 0 to −3 V on the same cell (sweep 5). Once the device reached an ON2 state, this state could be sustained under negative (sweep 6) and positive (sweep 7) voltage sweeps. Each state could be safely read by a small voltage (−0.5 V) for at least 10,000 s (Figure 4(c)) and by pulse (−1 V) reading for more than 10^6 cycles without obvious degradation (Figure 4(d)). Other M-DABDT-based devices (M: Zn, Cu, Ni, Pt) could also perform similar memory behaviours.

Device reproducibility is critical for potential industrial application, thus 50 devices for each kind of 1D CCP were measured and key statistical data are shown in Figure 5. The averaged first/second threshold voltages were between −1–

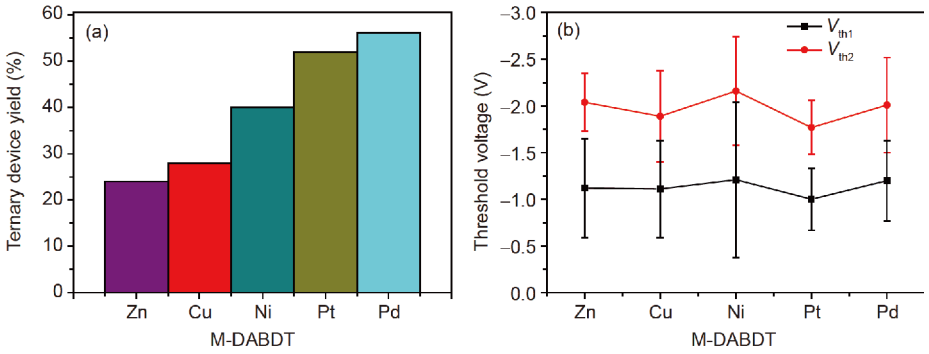

Figure 5 (a) Ternary device yield and (b) average threshold voltages (V_{th1} and V_{th2}) of M-DABDT based memory devices on a batch of fifty devices (color online).

−1.4 V/ −1.8–−2.2 V. The threshold voltages of memory devices based on 1D CCPs were lower than those of organic molecule-based RRAM devices [17,36–39], contributing to lower power consumption in use. Although Zn-/Cu-DABDT-based devices exhibited ternary memory behaviours, their ternary device yields were low (<30%), while for Ni-/Pt-/Pd-DABDT-based devices, the higher ternary device yields (≥40%) were achieved.

Many mechanisms have been proposed by which to explain memory switching behaviours, including conductive metal filament formation and charge trapping. A LiF layer (10 nm) was deposited between the active layer and Al electrode to examine the possibility of Al filament formation. This LiF layer could prohibit penetration of Al. The ITO/M-DABDT/LiF/Al structure memory devices could still exhibit ternary memory behaviours (Figure S17), ruling out the formation of aluminium filaments. To understand the differences in memory performance and the mechanism underpinning such resistance switching, we plotted the log(I)-log(V) curve of a typical ternary device (Figure 6(a)) and proposed that the first, and second resistance switches occurred in accordance with the space charge limited current (SCLC) model [40–43] and grain boundary depletion limited current (GBLC) model [44–47], respectively. The two

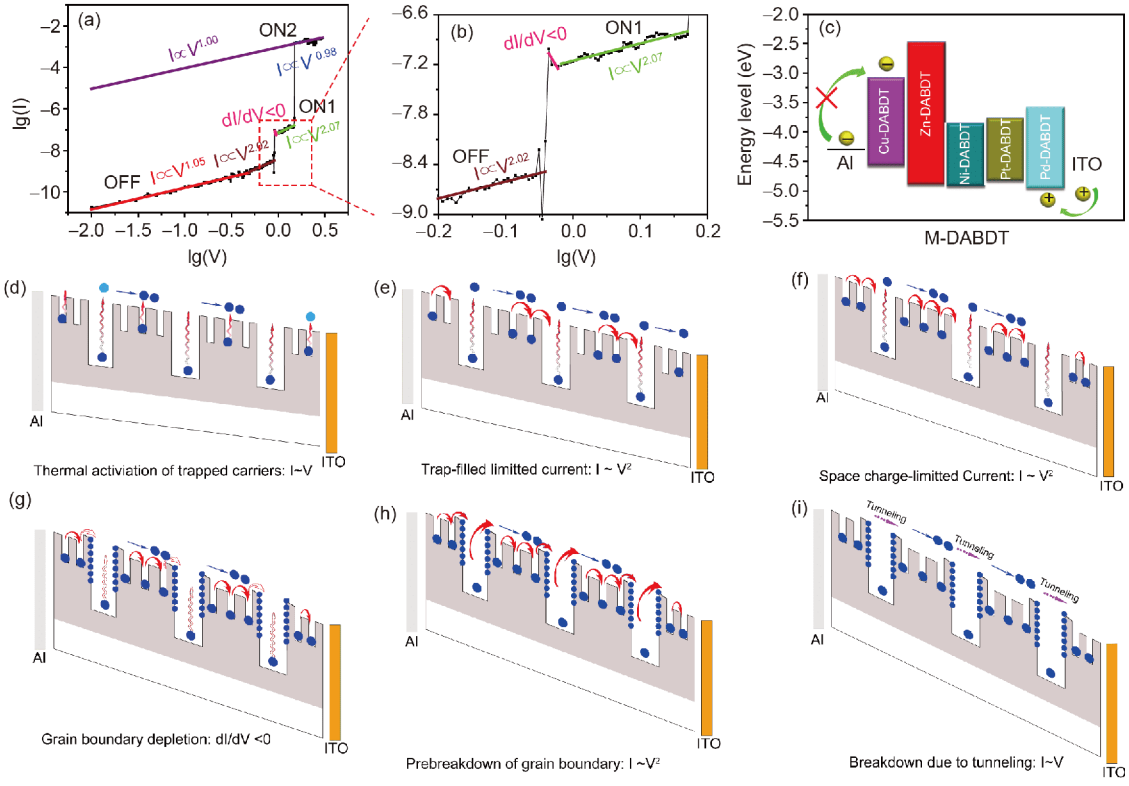

Figure 6 Current-voltage (I-V) relationship in log-log plot of (a) Pd-DABDT-based device and (b) enlarged curve of dI/dV<0 region; (c) energy diagram of M-DABDT 1D CCPs calculated from UV-Vis spectra and cyclic voltammograms; (d–i) transportation mechanism of charge carriers from low conductive state to intermediate conductive state and further to high conductive state (color online).

models have been described in a previous study. Briefly, throughout the ternary memory writing process, six physical conduction models are involved. The traps in the film could trap free charge carriers during transportation. Here the charge carriers were holes because the hole injection barriers were much smaller than the electron injection barriers (Figure 6(c)). At low electric field, the transported charge carriers mainly comprised those carriers generated from thermal excitation of the filled traps, therefore a low conductivity state was first observed and the conductivity obeys Ohmic behaviour (I-V, Figure 6(d)). As the electrical field gradually increases, the traps in our 1D CCP films were gradually filled, causing the Fermi level to approach the conductive band, whereupon the behaviour followed a square law (I-V^2) caused by the trap-filled limited current (TFLC, Figure 6(e)) [48]. As the electric field approaches the first threshold voltage (V_{th1}), all of the traps in the grains were filled up, the conductivity jumps to the higher level, and the square law (I-V^2) prevails. At this moment, the behaviour follows the SCLC model (Figure 6(f)) [40,42,48]. Besides the traps in the grains, charge carriers also need to overcome the barrier arising from the accumulation of impurities and disoriented crystalline structures at grain boundaries to hop to neighbouring grains [48]. Therefore, charge carriers will be trapped here and will form double depletion layers (grain boundary depletion), increasing the energy barriers further and resulting in a negative differential current ($dI/dV<0$, Figure 6(g)) [48]. As the electric field further increases, the barrier caused by the double depletion layers will be effectively reduced and the current will rapidly increase (grain boundary limited current, GBLC, Figure 6(h)). Once the electric field grows enough, the carriers could tunnel across grain boundaries directly (Figure 6(i)), leading to a linear I-V relationship.

Under the aforementioned mechanism, discrepancies in memory performance of the five types of devices could be interpreted. According to Marcus transport theory for organic materials [29–31], given similar crystalline structures, a narrower bandgap could offer a significantly higher carrier hopping rate and become more conductive. For Ni-/Pt-/Pd-DABDT CCPs, they have much smaller band gaps than the other two CCPs. Charge carriers could be transported much more efficiently and the formation of the conductive channels in the film will become easier. Therefore, Ni-/Pt-/Pd-DABDT based devices offer a higher ternary device yield.

Since Ni-/Pt-/Pd-DABDT CCPs have similar band gaps, crystallinity will play a subtle role in affecting memory performance. When a voltage was applied to the device, charge carriers need to overcome structural defects such as grain boundaries, which would require that additional energy arising only from a greater electrical field strength. Given too much electrical loss, the residual electrical field may be too small to fill the deep traps [15,49]. Among Ni-/Pt-/Pd-DABDT CCPs, Pd-DABDT CCP has the best crystallinity. Under the same external voltage/electric field, Pd-DABDT CCP will reserve the largest proportion of the electrical field strength for memory switching: this will induce more ternary memory switching, leading to the highest ternary device yield. Contrarily, for Ni-/Pt-DABDT CCPs, more severe molecular accumulation caused more electrical loss, finally resulting in a lower ternary device yield. In short, by designing a 1D-CCP with a more planar conjugation chain, a smaller band gap, and better crystallinity, the low ternary device yield and diverse voltage distribution of RRAMs could be prevented.

4 Conclusions

In conclusion, five 1D conjugated coordination polymers were synthesised in a solution process and fabricated into RRAM devices. The ternary device yield could be improved from 24% to 56% by altering the central metal ions of the coordination polymers. Ni-/Pt-/Pd-DABDT-based devices had higher ternary device yields than the other two owing to their planar chains and lower band gaps, causing more efficient charge transportation in such films. In addition, for a Pd-DABDT-based memory device, the better crystallinity resulted in less electrical loss at defects, resulting in the highest ternary device yield. Although the performance of 1D-CCP-based memory devices cannot completely meet the requirements for industrialisation, our results revealed that the planar conjugation chain, smaller band gaps, and improved crystallinities play important roles in the optimisation of the performance of ternary RRAM devices fabricated from lower-dimensional hybrid materials.

Acknowledgements This work was supported by the National Natural Science Foundation of China (21603158, 21336005), the Major Research Project of Natural Scientific Research Foundation of the Higher Education Institutions in Jiangsu Province (15KJA150008, 17KJA150010), Suzhou Science and Technology Bureau Project (SYG201524), and the Priority Academic Program Development of Jiangsu Higher Education Institutions.

Conflict of interest The authors declare that they have no conflict of interest.

Supporting information The supporting information is available online at http://chem.scichina.com and http://link.springer.com/journal/11426. The supporting materials are published as submitted, without typesetting or editing. The responsibility for scientific accuracy and content remains entirely with the authors.

1 Cheng XF, Hou X, Zhou J, Gao BJ, He JH, Li H, Xu QF, Li NJ, Chen DY, Lu JM. *Small*, 2018, 14: 1703667
2 Gu C, Lee JS. *ACS Nano*, 2016, 10: 5413–5418
3 Liu Y, Wang H, Shi W, Zhang W, Yu J, Chandran BK, Cui C, Zhu B, Liu Z, Li B, Xu C, Xu Z, Li S, Huang W, Huo F, Chen X. *Angew Chem Int Ed*, 2016, 55: 8884–8888
4 Ma Y, Cao X, Li G, Wen Y, Yang Y, Wang J, Du S, Yang L, Gao H,

Song Y. *Adv Funct Mater*, 2010, 20: 803–810
5 Ielmini D. *Semicond Sci Technol*, 2016, 31: 063002
6 Li H, Xu Q, Li N, Sun R, Ge J, Lu J, Gu H, Yan F. *J Am Chem Soc*, 2010, 132: 5542–5543
7 Li Y, Chen L, Ai Y, Hong EYH, Chan AKW, Yam VWW. *J Am Chem Soc*, 2017, 139: 13858–13866
8 Liu Y, Liu Z, Zhu B, Yu J, He K, Leow WR, Wang M, Chandran BK, Qi D, Wang H, Chen G, Xu C, Chen X. *Adv Mater*, 2017, 29: 1701780
9 Li Y, Zhang C, Gu P, Wang Z, Li Z, Li H, Lu J, Zhang Q. *Chem Eur J*, 2018, 24: 7845–7851
10 Wang C, Hu B, Wang J, Gao J, Li G, Xiong WW, Zou B, Suzuki M, Aratani N, Yamada H, Huo F, Lee PS, Zhang Q. *Chem Asian J*, 2015, 10: 116–119
11 Gu PY, Gao J, Lu CJ, Chen W, Wang C, Li G, Zhou F, Xu QF, Lu JM, Zhang Q. *Mater Horiz*, 2014, 1: 446–451
12 Li Y, Wang Z, Zhang C, Gu P, Chen W, Li H, Lu J, Zhang Q. *ACS Appl Mater Interfaces*, 2018, 10: 15971–15979
13 Chen H, Wu L, Xiao X, Wang H, Jiang J, Wang L, Xu Q, Lu J. *Sci China Chem*, 2017, 60: 237–242
14 Cheng XF, Xia SG, Hou X, Xiao X, He JH, Ren ZG, Xu QF, Li H, Li NJ, Chen DY, Lu JM. *Adv Mater Technol*, 2017, 2: 1700202
15 Cheng XF, Hou X, Qian WH, He JH, Xu QF, Li H, Li NJ, Chen DY, Lu JM. *ACS Appl Mater Interfaces*, 2017, 9: 27847–27852
16 Hou X, Cheng XF, Xiao X, He JH, Xu QF, Li H, Li NJ, Chen DY, Lu JM. *Chem Asian J*, 2017, 12: 2278–2283
17 Hou X, Xiao X, Zhou QH, Cheng XF, He JH, Xu QF, Li H, Li NJ, Chen DY, Lu JM. *Chem Sci*, 2017, 8: 2344–2351
18 Liu SJ, Wang P, Zhao Q, Yang HY, Wong J, Sun HB, Dong XC, Lin WP, Huang W. *Adv Mater*, 2012, 24: 2901–2905
19 Zhang Q, He J, Zhuang H, Li H, Li N, Xu Q, Chen D, Lu J. *Adv Funct Mater*, 2016, 26: 146–154
20 Hong EYH, Poon CT, Yam VWW. *J Am Chem Soc*, 2016, 138: 6368–6371
21 Song S, Ko YG, Lee H, Wi D, Ree BJ, Li Y, Michinobu T, Ree M. *NPG Asia Mater*, 2015, 7: e228
22 Cheng XF, Shi EB, Hou X, Shu J, He JH, Li H, Xu QF, Li NJ, Chen DY, Lu JM. *Adv Electron Mater*, 2017, 3: 1700107
23 Bin Z, Li J, Wang L, Duan L. *Energy Environ Sci*, 2016, 9: 3424–3428
24 Li Y, Li H, Chen H, Wan Y, Li N, Xu Q, He J, Chen D, Wang L, Lu J. *Adv Funct Mater*, 2015, 25: 4246–4254
25 Lu G, Tang H, Huan Y, Li S, Li L, Wang Y, Yang X. *Adv Funct Mater*, 2010, 20: 1714–1720
26 Shirota Y. *J Mater Chem*, 2000, 10: 1–25
27 Shirota Y. *J Mater Chem*, 2005, 15: 75–93
28 Sivula K, Luscombe CK, Thompson BC, Fréchet JMJ. *J Am Chem Soc*, 2006, 128: 13988–13989
29 Geng H, Peng Q, Wang L, Li H, Liao Y, Ma Z, Shuai Z. *Adv Mater*, 2012, 24: 3568–3572
30 Marcus RA. *J Chem Phys*, 1956, 24: 979–989
31 Marcus RA. *J Chem Phys*, 1956, 24: 966–978
32 Hu X, Yu D. *RSC Adv*, 2012, 2: 6570–6575
33 Aasmundtveit KE, Samuelsen EJ, Guldstein M, Steinsland C, Flornes O, Fagermo C, Seeberg TM, Pettersson LAA, Inganäs O, Feidenhans'l R, Ferrer S. *Macromolecules*, 2000, 33: 3120–3127
34 Ungár T. *Scripta Mater*, 2004, 51: 777–781
35 Zhokhavets U, Erb T, Gobsch G, Al-Ibrahim M, Ambacher O. *Chem Phys Lett*, 2006, 418: 347–350
36 Cheng XF, Shi EB, Hou X, Xia SG, He JH, Xu QF, Li H, Li NJ, Chen DY, Lu JM. *Chem Asian J*, 2017, 12: 45–51
37 Gu PY, Zhou F, Gao J, Li G, Wang C, Xu QF, Zhang Q, Lu JM. *J Am Chem Soc*, 2013, 135: 14086–14089
38 Su Z, Zhuang H, Liu H, Li H, Xu Q, Lu J, Wang L. *J Mater Chem C*, 2014, 2: 5673–5680
39 Zhang Q, Zhuang H, He J, Xia S, Li H, Li N, Xu Q, Lu J. *J Mater Chem C*, 2015, 3: 6778–6785
40 Rose A. *Phys Rev*, 1955, 97: 1538–1544
41 Lampert MA. *Phys Rev*, 1956, 103: 1648–1656
42 Mark P, Helfrich W. *J Appl Phys*, 1962, 33: 205–215
43 Xia Y, He W, Chen L, Meng X, Liu Z. *Appl Phys Lett*, 2007, 90: 022907
44 Dimos D, Chaudhari P, Mannhart J, Legoues FK. *Phys Rev Lett*, 1988, 61: 219–222
45 Hu H, Krupanidhi SB. *J Mater Res*, 1994, 9: 1484–1498
46 Wang G, Yang Y, Lee JH, Abramova V, Fei H, Ruan G, Thomas EL, Tour JM. *Nano Lett*, 2014, 14: 4694–4699
47 Yang JK, Kim WS, Park HH. *Thin Solid Films*, 2000, 377-378: 739–744
48 Chiu FC. *Adv Mater Sci Eng*, 2014, 2014: 578168
49 Li Y, Li H, He J, Xu Q, Li N, Chen D, Lu J. *Chem Asian J*, 2016, 11: 906–914